Modeling of the shot peening of a nickel alloy with the consideration of both residual stresses and work hardening

J.P. Goulmy [a], [*], V. Boyer [b], D. Retraint [b], P. Kanoute [c], L. Toualbi [c], E. Rouhaud [b]

[a] *Arts et Metiers Institute of Technology, MSMP, HESAM Université, F-13617 Aix-en-Provence, France*
[b] *Laboratoire des Systèmes Mécaniques et d'Ingénierie Simultanée (LASMIS), Université de Technologie de Troyes (UTT), 10000 Troyes, France*
[c] *Onera - The French Aerospace Lab, Département Matériaux et Structures, F-92322 Châtillon, France*

ARTICLE INFO

ABSTRACT

Shot peening of turbine disk engines is performed in the aerospace industry in order to enhance fatigue life. This surface enhancement method generates beneficial modifications like superficial compressive residual stresses that are known to delay crack initiation and propagation. In the same way, work hardening is also introduced at the surface of the part during shot peening and can have a significant influence on fatigue crack initiation. Taking this parameter into account in the fatigue design of parts, in addition to the residual stresses, is a real challenge to be the most predictive. One possibility for this is to be able to predict it during the modeling of the shot peening process. In the present work, various peening conditions are considered in order to be able to propose a model able to account for the influence of coverage and Almen intensity on residual stresses and work hardening. The studied material is Inconel 718, commonly used for aeronautical parts. The X-ray diffraction method is used to obtain the in-depth residual stress and work hardening profiles. A three-dimensional numerical model is proposed to predict these quantities. Efforts are made to consider all recent advances in three-dimensional simulation of the process, in terms of coverage assessment, shot and treated part modeling. The numerical results are compared to the experimentally measured residual stresses and work hardening.

1. Introduction

Shot peening is a surface enhancement process used to enhance fatigue life. It generates, in particular, compressive superficial residual stresses that prevent crack initiation and delay their propagation. This process is widely used in the aerospace industry to increase safety factors, but is seldom taken into account in the dimensioning step because its mastering remains often empirical. In fact, it is still difficult to estimate precisely the benefits of shot peening. During shot peening, the treated material is subjected to a complex mechanical load. The repeated impacts and the high velocity activate hardening mechanisms (isotropic and kinematic hardening) associated with the strain rate sensitivity of the treated material. It is clear now that the residual stress field is not the sole parameter that influences fatigue life. Work hardening is also an issue and has been identified as an influential parameter for fatigue resistance and residual stress relaxation by Prevey et al. (1998), Prevey (2000). This last point represents a major challenge for future developments because most of the current models are mainly interested in the accurate modeling of residual stresses, with little atten-

tion to the generated plastic strain and hardening effects. Consequently, an advanced understanding of the process and material behavior followed by realistic modeling is necessary to quantify shot peening benefits and improve the design of the relevant parts.

A clear and detailed literature review of shot peening models has been proposed by Zimmermann et al. (2010). These models can be divided into two groups: analytical and numerical models. The main advantage of analytical models is the rapid estimation provided for systems with simple geometry. On the other hand, they do not allow the study of complex issues such as the influence of hardening effects. Numerical models are more compliant, allowing many process parameters to be considered. Moreover, finite-element simulations have great potential for the analysis of stress and work hardening development while taking into account complex material behavior. Dealing with process parameters, Guagliano et al. proposed a numerical approach to link the Almen intensity to the residual stress field after shot peening (Guagliano, 2001). Hasegawa et al. (1996) and Kobayashi et al. (1998) experimentally demonstrated that static and dynamic indentations lead to different results. Such observations were confirmed by local indenta-

Table 1
Composition of the Inconel 718 DA Alloy provided by the manufacturer (Wt%).

Ni	Fe	Cr	Mo	Al	Ti	Nb	Si	C
54.18	17.31	17.97	2.97	0.56	1	5.39	0.1	0.023

Table 2
Overview of the experimental shot peening conditions investigated. The cells with a grey background correspond to the conditions that have also been investigated numerically (see Section 6).

Almen Intensity	Coverage (%)				
F8-9A	-	-	200	-	-
F12-13A	65	125	200	320	400
F17-18A	–	–	200	–	–
F22-23A	65	125	200	320	400

tion studies performed by Kermouche et al. (2013), Al Baida et al. (2015). Using an elasto-visco-plastic model, Zimmermann et al. could successfully predict the residual stress state after shot peening, so did Klemenz et al. (2009). Surface roughness was also assessed by Bagherifard et al. (2012a) and Mylonas and Labeas (2011). Bagherifard's literature review (Bagherifard et al., 2012b) shows that various strategies were proposed to follow the evolution of coverage by numerical means, based on plastic threshold (Gangaraj et al., 2014) or random position of shot (Miao et al., 2009). Shot material influence has been investigated by Mori et al. (1996), Rouhaud and Deslaef (2002) and Meguid et al. (2002). More recently, new models have been proposed in the literature on different materials, showing the interest in predicting correctly the mechanical fields. Maliaris et al. proposed a FEM-based 2D model to simulate the shot peening process of 51CrV4 steel (Maliaris et al., 2021). Zhao et al. have investigated the effects of the process parameters, initial surface morphology and initial residual stress on the residual stress distribution after shot peening by using a finite element model of 12Cr2Ni4A steel (Zhao et al., 2022). Zhou et al. proposed a FEM-based 3D model to simulate the shot peening process of different steels by considering different types of modeling parameters (Zhou et al., 2022; Zhou and Sun, 2022).

One of the key points for a successful model of the mechanical fields after shot peening concerns the choice of the constitutive model for the treated material. Shot peening is a cyclic process performed at a wide range of strain rates. Different models have been proposed to translate the behavior of the material during the process. In order to take into account visco-plastic effects, Johnson-Cook or power law models are generally considered (Al-Hassani, 1981; ElTobgy et al., 2004; Majzoobi et al., 2005). However, as detailed by Baragetti, these models consider only isotropic hardening and lead to an overestimation of compressive residual stresses (Baragetti, 2001). Using an elasto-visco-plastic model, Zimmermann et al. have successfully described the compressive residual stress state in IN718 nickel-based alloy.

The non-exhaustive literature review proposed above shows the great potential of such numerical models. If predictive results in terms of residual stress fields are now proposed in the literature, work hardening is hardly assessed, when it has been experimentally proven by Prevey that work hardening plays an important role in stress relaxation (Prevey, 2000). It seems, therefore, essential to validate shot peening models with respect to this parameter as well. Models including accurate predictions of both the residual stress field and the hardening state could then be used as initial states in fatigue models for a better assessment of fatigue life.

The objective of this paper is thus to propose a numerical model to predict both residual stresses and work hardening profiles induced by shot peening. First, an extended experimental campaign has been set up to study the influence of Almen intensity and coverage on both residual stresses and work hardening. Then, a 3D finite-element model of the

process is proposed, considering an elasto-visco-plastic behavior for the material. Special attention is paid to the coverage evaluation and the shot model. In section 4, numerical results are exposed and commented upon. Finally, the model is validated by comparing the results with experimental data.

2. Material and methods

2.1. Material and shot peening conditions

An Inconel 718 Direct Aged (IN718 DA) nickel-based alloy has been investigated in this work. The composition is given in Table 1. This alloy is widely used in the aerospace industry because it exhibits excellent mechanical properties at high temperature. The Direct Aged metallurgical state is obtained by direct quenching after forging, i.e. no recovery at high temperature but precipitation treatment at 720 °C and 620 °C for the strengthening phases. The IN718 DA is then composed of four different phases: the matrix γ, the strengthening precipitates γ' and γ'', and the δ phase.

Parallelepipedic samples of $15 \times 15 \times 10$ mm³ have been machined from a turbine disc made of IN718 DA. Prior to any shot peening treatments, all samples have been mechanically polished to a mirror state in order to remove as much as possible residual stresses and work hardening induced by machining: XRD measurements have been carried out to verify that the samples are free of residual stresses and work hardening (see section 2.3).

Based on standard treatments used in industry, a large set of shot peening conditions has been considered to investigate the influence of coverage and intensity on the resulting stress and hardening states. A conventional shot peening nozzle and S110 steel shot were used to perform the surface treatment. The various process parameters chosen for the experimental campaign are gathered in Table 2. On the one hand, two shot peening intensities, *F12-13A* and *F22-23A*, have then been investigated for five different values of coverage (*65 %, 125 %, 200 %, 320 %* and *400 %*). The Almen intensity is established according to the NFL 06–832 standard and is expressed in hundredths of millimeters (Norme AFNOR NFL 06-832, 1990).

On the other hand, coverage has been set at *200 %* and four shot peening intensities have been studied (*F8-9A, F12-13A, F17-18A* and *F22-23A*). Experimental coverage has been visually assessed, following SAE standard J2277 (J2277: Shot Peening Coverage Determination - SAE International, n.d.). The coverage that is experimentally applied is generally higher than 100 %. However, in order to test the ability of the model to predict an intermediate state and not only a saturated state, it is proposed to characterize the residual stresses and work hardening for a coverage of 65 %.

2.2. Material characterization

Residual stress and work hardening levels have been evaluated using X-ray diffraction (XRD). The residual stress intensity has been evaluated with the classical $\sin^2\psi$ method; the work hardening levels have been evaluated with diffraction peak width determination (François and Lebrun, 1992; François et al., 1995). A four-circle Seifert PTS diffractometer equipped with a PSD detector and a Co tube (λCo-Kα = 1.79 Å) have been used to perform all the measurements on the 311 diffraction peak ($2\theta \approx 111°$). An accelerating voltage of 20 kV and a current of 4 mA have been chosen. Eleven ψ angles ranging from $-60°$ to 60° have been used both for residual stress measurements and the determination of the full width at half maximum (FWHM) of Pseudo-Voigt profile fits. Under these conditions, the X-ray penetration depth is estimated to vary between 2 and 4 μm. To perform the in-depth XRD measurements, successive material removals have been carried out by electrolytic polishing using a solution of 70 % (vol) ethanol, 20 % perchloric acid and 10 % propylene glycol monomethyl. The thickness of the
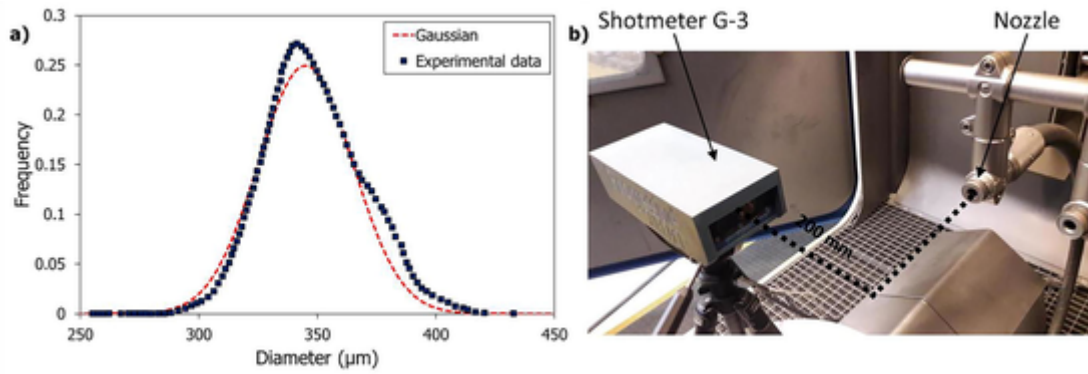
Fig. 1. a) Dispersion of the shot diameter fitted with a Gaussian distribution. The average diameter is 345 μm with a standard deviation of 20 μm. b) Shotmeter sensor positioning for shot velocity measurement of the shot stream.
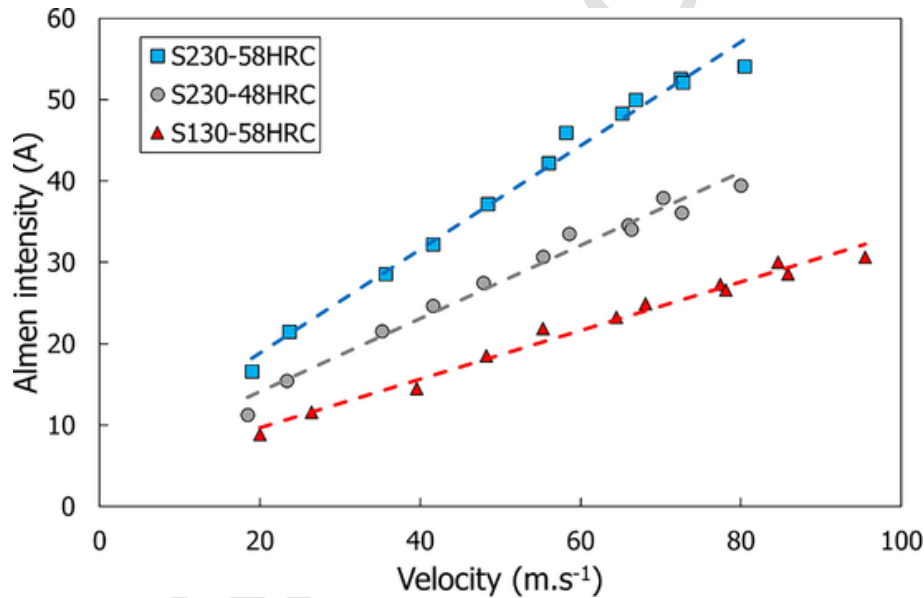

Fig. 2. Evolution of the Almen intensity as a function of shot velocity for three types of shot (experimental values).

removed material layer has been measured by a coordinate measuring machine. The uncertainty on the x-axis corresponds to the errors due to the electrolytic polishing procedure and those due to the X-ray penetration. It can be estimated to be of the order of 10 μm. The layer removal impact has been taken into account in the residual stress measurements, but the established correction procedure revealed that this impact is negligible in the conditions of this study. Residual stresses and peak widths have been measured in two directions. However, no significant differences were revealed, confirming that shot peening introduces an in plane equi-biaxial stress state. A measurement in one direction is thus sufficient to assess the mechanical state of each part.

2.3. Experimental assessment of the process

The objective of this section is to describe the approach used to establish the values of the process parameters, and the distribution of their variations that are necessary for an accurate simulation of the process. Indeed, each of these parameters may affect the residual stress and work hardening profiles significantly. Also, many parameters related to the shot stream are subjected to variations. These variations occur during the stream flow itself.

A single type of shot (S130-58HRC) has been used to perform all the shot peening treatments using the same shot peening machine. Experimental measures of the size of the shot have been conducted on a batch

of shots used for the shot peening treatment of the samples. The distribution of the shot diameters is presented in Fig. 1.a. It has been approximated with a Gaussian function having an average of 345 μm and a standard deviation of 20 μm.

To obtain the shot velocity, the shot peening-intensity was translated in terms of average shot velocity based on the work of Miao et al. (2009). The average shot velocity has also been measured using a Shotmeter G-3 measurement tool. This device consists of a sensor and a controller connected to a computer. The sensor has been placed perpendicular to the shot flow at a distance of 200 mm from the nozzle (see Fig. 1.b).

To validate the method, this study has been conducted for three types of shots (S230-58 HRC, S230-48HRC and S130-58HRC). Fig. 2 presents the Almen intensity as a function of the measured average velocity for the three types of shot. A linear relationship is observed between the Almen intensity and the velocity for the three shot types. The red curve corresponds to the S130-58HRC shot, the shot that has been used in the present study. Each of the Almen intensities used to treat the samples (see Table 2) may then be correlated with an average shot velocity (see Table 3).

Using particle tracking velocimetry, Kubler et al. (2020) have shown that the positions of the large number of impacts on the part during a shot peening treatment could be treated as a random variable. In order to confirm these results, an optical microscopy characterization was

Table 3

Correlation between Almen intensities and average shot velocities for S130-58HRC shot.

Intensity	F8-9A	F12-13A	F17-18A	F22-23A
Velocity (m.s^{-1})	17	35	50	65

performed for samples shot peened with Almen intensity *F12-12A* and *F22-23A* and for different coverages (Fig. 3). The analyses of the treated surface confirm that the shot impacts can be observed on the surface after shot peening; the distribution of the positions of these impacts can be modelled with a normal distribution (Table 4).

2.4. Work hardening evaluation

The calibration procedure proposed by Goulmy et al. has been used (Goulmy et al., 2021b, 2021a) in order to evaluate the amount of work hardening introduced during shot peening. This methodology has previously been successfully applied to IN718 DA and is briefly summarized in the following paragraph.

To establish this calibration methodology, several loading conditions have been investigated, including single tension, single compression, high strain rates and low cycle fatigue. Three experimental techniques have been used to characterize the work hardening on the deformed samples: microhardness, X-ray diffraction (XRD) and Electron Backscatter Diffraction (EBSD). The experimental tests were also simulated with a pertinent elasto-visco-plastic model. The correlation between the model variables and the experimental parameters (FWHM, KAM and micro-hardness) enabled to choose the equivalent plastic strain ε^p as a model variable representative of work hardening. The equivalent plastic strain is defined by:

$$\varepsilon^p = \sqrt{\frac{2}{3}\varepsilon^p : \varepsilon^p} \tag{1}$$

where ε^p is the plastic deformation tensor.

The results revealed that the equivalent plastic strain is well correlated with the FWHM of XRD peaks and that it is necessary to take into account the strain rate to construct the correlation curves.

Fig. 4 presents the resulting correlation curves (Goulmy et al., 2021b, 2021a), taking into account the strain rate, the loading history and the temperature for an IN718 DA. Fig. 4 shows that the FWHM increases with plastic strain; the evolution is not linear and the shape of the curve is similar for the two strain rates. The strain rate has a stronger influence on higher plastic strain levels: between 10 and

40 % of plastic strain, the FWHM is 10 % lower for a strain rate of 10^{-3} s^{-1} compared to the one obtained for 10^3 s^{-1}.

3. Experimental results

The residual stress and work hardening profiles obtained on samples treated with different shot peening conditions are presented in this section. The work hardening profiles have been evaluated with the calibration curve corresponding to the strain rate of 10^{-3} s^{-1} for all the process parameters treated in this study and gathered in Table 2; these experimental results are presented in Fig. 5 and Fig. 6 of the present section. The work hardening profiles have also been evaluated for a strain rate of 10^3 s^{-1} for all the process parameters that have been the object of a numerical model (the gray cells in Table 2); the corresponding experimental results are presented in Section 6 (Fig. 16 to Fig. 18). Note that the grain size and the size of the precipitates are not modified during the different shot peening treatments studied in this work, as observed by Goulmy et al. (2021a).

3.1. Influence of Almen intensity

The influence of Almen intensity ranging from *F8-9A* and *F22-23A* has been studied on the residual stress and work hardening profiles. The results are presented in Fig. 5 for a coverage of *200 %*. Before shot peening, the samples presents slight tensile residual stresses of around 150–200 MPa, roughly constant at least up to a depth of 200 μm (Fig. 5.a). The level of work hardening before shot peening is close to zero and constant in-depth (Fig. 5.b). As far as residual stresses are concerned, the main differences between the different profiles lie in the depth affected by compressive stresses as well as the depth at which the residual stresses become equal to zero: the higher the peening intensity, the deeper the maximum compressive residual stresses and the thicker the area affected by the compressive residual stresses (Fig. 5.a). Little influence can be observed on the maximal compressive residual stress value, which varies from −1100 MPa for the strongest intensity to −1000 MPa for the lowest intensity. Work hardening is strongly dependent on the shot peening intensity. It is interesting to note in Fig. 5.b that work hardening decreases rapidly in-depth to reach a constant low value (below 3 %) above 100 μm. Besides, the higher the shot peening intensity, the greater the work hardening at a given depth between 0 and 100 μm.
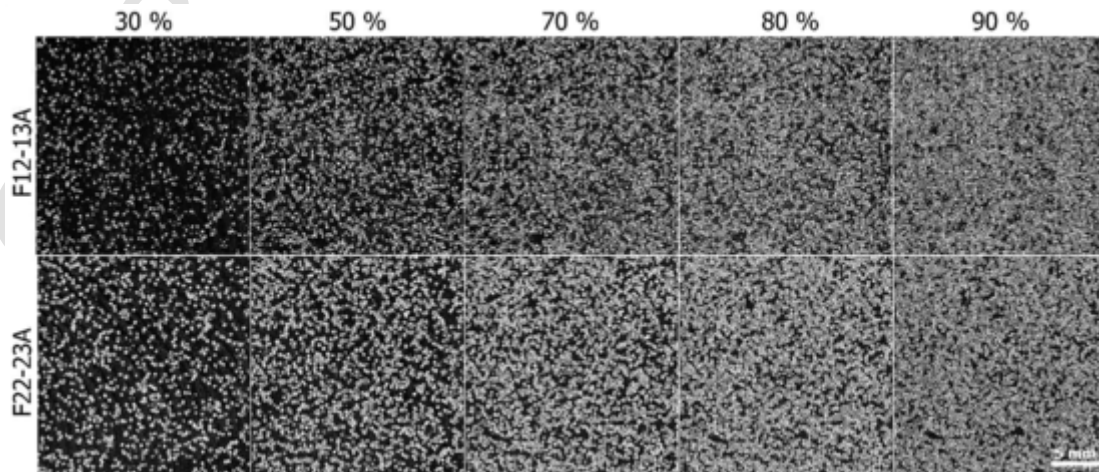

Fig. 3. Characterization of impacts generated during shot peening with Intensities F12-13A and F22-23A for varying coverages. Non-impact area appears in black on the micrographs.

Table 4
Identified parameters for the constitutive model of IN718 DA.

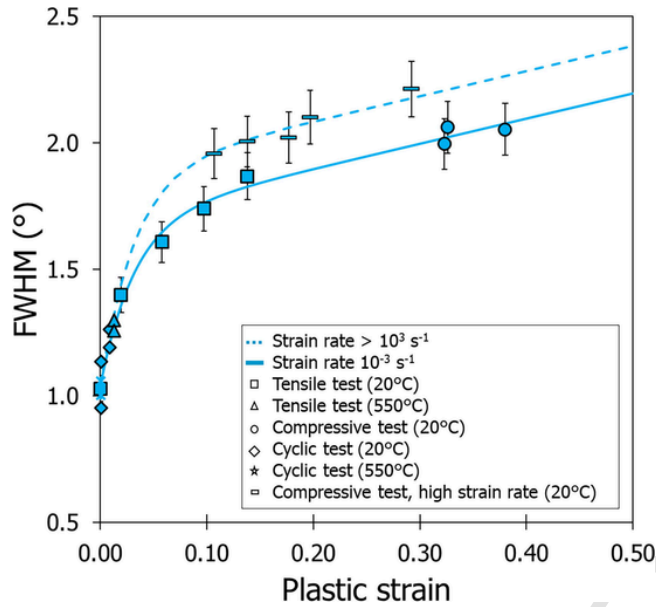| E (MPa)	ρ (kg.m^{-3})	ν	K (MPa)	n	R (MPa)	Q (MPa)	b	C_1	C_2	C_3	D_1	D_2	D_3
204,000	8400	0.3	80	5.31	700	−215	−3	4.7 10^5	9.0 10^3	2.4 10^3	1000	100	10

Fig. 4. FWHM as a function of the equivalent plastic strain for several loading history, temperature, strain rates with the respective calibration curves for IN-718 DA (Goulmy et al., 2021b).

3.2. Coverage influence

The influence of a coverage ranging from *65 %* to *400 %* has been studied on the mechanical state of IN718 DA. Fig. 6.a and Fig. 6.b presents residual stress and work hardening profiles as a function of coverage for an intensity of *F12-13A*. The maximum compressive residual stress fluctuates slightly around a value of −850 MPa for up to *125 %* coverage and then stabilizes at a value of −1100 MPa from a coverage value of *200 %*. It is located at a depth of around 50 μm, whatever the coverage value is considered. All coverages lead to a similar affected depth that lies between 130 and 150 μm. Surface work hardening values are strongly dependent on coverage. At a given depth in the work hardened layer, the higher the coverage between *65 %* and *320 %*, the greater the work hardening. On the other hand, no significant difference can be observed between the work hardening profile obtained for a coverage value of *320 %* and the one at *400 %*. This result implies that work hardening evolves much less significantly above a certain coverage value. Then, the work hardening reaches very low values (inferior to 3 %) beyond 100 μm depth, comparable to the values found in the untreated material, regardless of the coverage.

Fig. 6.c and Fig. 6.d presents residual stress and work hardening profiles as a function of coverage for an Almen intensity of *F22-23A*. All stress profiles appear very similar, whatever the coverage value. The top superficial residual stress value as well as the maximum compressive residual stress value are comparable to the values obtained with an Almen intensity of *F12-13A*. The main difference in the stress profiles is the depth at which the maximum compressive stress occurs: around 90–100 μm in the latter case versus a lower value of 50 μm for the lowest Almen intensity case. Similarly, the depth at which the stress value reaches zero is at a greater depth, close to 220 μm compared to 150 μm in the previous case. Regarding the evolution of the work hardening with the coverage at this shot peening intensity, the profiles are very comparable for all studied coverage values. Only the extreme surface

values differ slightly: the higher the coverage, the higher the extreme surface value with a stagnation from a coverage of *200 %*. These results are similar to those obtained for a lower intensity. However, due to the higher shot peening intensity, the stagnation of work hardening as a function of coverage occurs at lower values of coverage.

4. Numerical model for shot peening

A numerical model is presented in this section to predict the mechanical state (both residual stresses and hardening levels) of the treated part after shot peening. It is a three-dimensional finite-element model of the process built using the commercial software ABAQUS Explicit 6.12.2. The model simulates multiple shot impacts on a material surface. Additional analyses using single-shot impact simulation have also been carried out, as needed, to validate specific features of the model.

The modeling of the shot peening process can be performed with either static or dynamic computation. In shot peening, inertial effects are negligible. It is then possible to make a static simulation for which the shot would have an initial condition in displacement and not in velocity. However, prior knowledge of the maximum penetration of the shot in the material is necessary. A dynamic algorithm was thus preferred here. The strong non-linearities of the problem, in particular due to the contact between the shot and the shot-peened material, impose very small time steps. An explicit algorithm has then been chosen. To assess the convergence of the model, the energy balance of the numerical simulation is systematically evaluated. An error of less than 5 % on the estimated total energy is the criterion defined to validate the convergence.

4.1. Model for the shot and contact

A single type of shot (S130-58HRC) has been used to perform all the shot peening treatments (see Section 3). The shot density is set to 7800 kg.m^{-3}, and it has been modelled with spheres that are meshed with C3D4 linear tetrahedron elements. The diameter of the shot has been set to a value of 345 μm, the average diameter of distribution determined on a batch of shots (see Fig. 1.a and Section 2.3).

A rigid model for the shot material is realistic when the elastic limit of the shot is significantly higher than that of the treated solid: a factor of 2 seems to be the minimum (Rouhaud and Deslaef, 2002). In the present case, the material to be treated has a particularly high yield strength, approaching 1400 MPa at 20 °C to be compared with 2000 MPa, the yield stress of the shot used in this work. As a consequence, modeling the shot as a perfect rigid body would not be realistic.

Simulations of single impacts have been carried out to establish whether the shot model should be elastic or elasto-plastic. The shot has been modelled with an elastoplastic material. The dissipated energy in the shot has been evaluated for different shot velocities and for different elastic limits of the shot and compared to the initial kinetic energy of the shot. It has then been observed that less than 10 % of this energy is converted into plastic work. As a consequence, it can be assumed that after a few impacts, due to hardening mechanisms, the shot has purely elastic behavior. This is confirmed by the fact that a very low level of damaged shot has been observed during the shot peening of the samples. Given the observations outlined above, the behavior of the shot has been considered elastic in the multiple shot impact simulations. The Young modulus has been set to 210 GPa and the Poisson ratio to 0.3.

In Section 2, it has been highlighted that it was possible to determine the average shot velocity as a function of Almen intensity (see
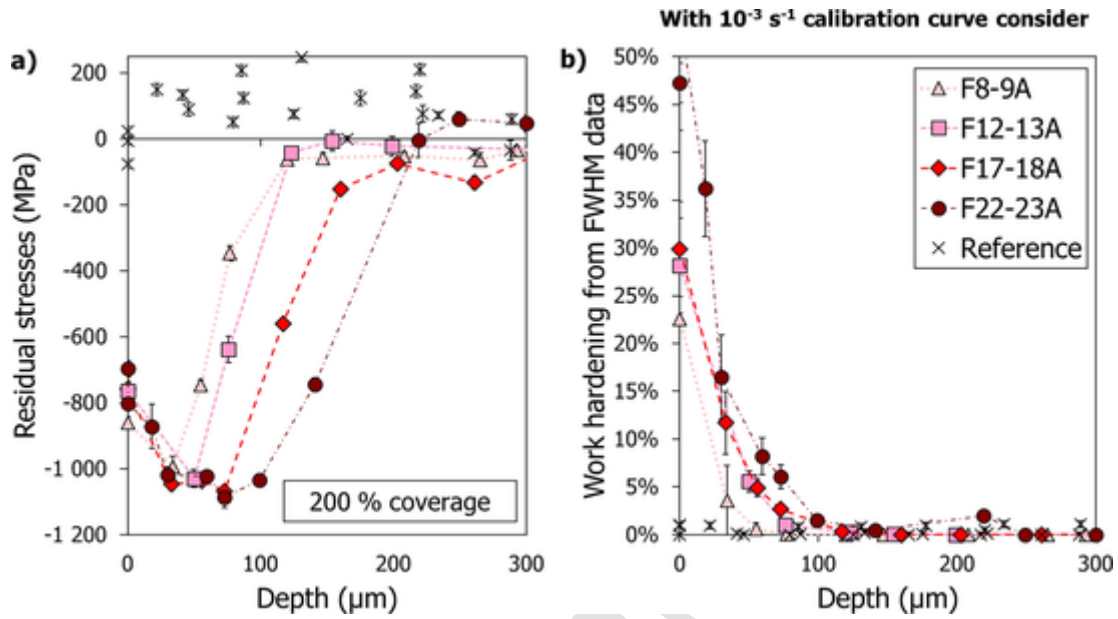
Fig. 5. Experimental residual stresses (a) and work hardening (b) profiles as a function of depth for various peening intensity and a fixed coverage of 200 %. Work hardening is calculated from the 10^{-3} s^{-1} calibration curve shown in Fig. 4.

Table 3). In the simulation of the multiple shot impacts, the value of the shot velocity has then been fixed to obtain the desired Almen intensity, according to the linear evolution presented in Fig. 2 and a normal incidence was considered for the shot.

The contact between the shot and the treated part is simulated using a hard contact algorithm with an isotropic Coulomb friction coefficient of 0.05. This value has been chosen on the basis of feedback from the CRED (Centre de Ressources en Essais Dynamiques) of the Ecole Centrale de Nantes. The influence of this parameter on the results has already been discussed by Mequid et al. and Kim et al. and is not addressed here (Meguid et al., 2002; Kim et al., 2012).

4.2. Model for the treated part

A cylinder was used to model the shot peened part. The mesh is composed of C3D8R elements with reduced integration and hourglass control. The displacement of the nodes located on the lateral surface and on the bottom base of the cylinder has been blocked in the direction of the normal to the corresponding surface. The geometry of the treated part and the boundary conditions are presented in Fig. 7. Several quantities have been defined to describe the geometry of the treated part: its thickness, noted T, the area of the shot-peened surface and the area of the surface of the part that is not treated. The width of the not shot peened surface is noted as W (see Fig. 7).

The dimensions of the treated part have to be chosen to ensure that the model is equivalent to the semi-infinite medium. The criteria for defining the appropriate dimensions that meet this assumption have received considerable attention in the literature (Gangaraj et al., 2014; Meguid et al., 1999). The dimensions are usually expressed as a function of R_s, the radius of the shot. A preliminary study for a single-shot impact under normal incidence has been conducted to set the values of the dimension of the model. The residual mechanical fields have then been evaluated for several thicknesses T of the part and widths W of the external area (NSPSA). The resulting residual stress fields have been analyzed along the depth as well as along the radius at the surface of the part. The results, presented in Fig. 8, show that the profile of the residual stress along the depth is independent of the thickness of the treated part model for the chosen thicknesses. On the other hand, the width of the external area needs to be at least equal to 5 times the shot radius R_s to obtain a stress state that is independent of the cylinder radius. The

chosen dimensions for the multiple shot impact simulations have finally been set to $T = 10R_s$ and $W = 5R_s$. This choice is coherent with the criteria proposed in the literature cited previously (Gangaraj et al., 2014; Meguid et al., 1999).

To complete these analyses, a specific study has also been conducted to determine the size of the shot peened surface (i.e., impacted surface) that is needed to obtain a representative mechanical state for a given simulation of a shot peening treatment. A surface radius of R_s, $1.5R_s$ and $2R_s$ has been tested considering multiple shot impact simulations. The best compromise has been reached for $1.5R_s$, as it will be illustrated later in Section 5. This result is again in accordance with the literature (Gangaraj et al., 2014).

The size of the mesh for the impacted area also requires some attention. The maximal representative length of an element needs to be kept under $D_p/20$ to ensure convergence, where D_p is the diameter of the dimple produced by a single impact (Bagherifard et al., 2014). This value depends on the shot velocity and thus on the Almen intensity (see Section 3). A specific study has thus been conducted to determine the minimal size that the elements should have. From single-shot impact simulations, the analysis of the resulting dimple diameter has led to the setting of the size of the smallest element at 6 μm.

4.3. Constitutive model for the shot-peened material

The behavior of Inconel 718 has been extensively investigated (Alexandre et al., 2004; Chaboche and Jung, 1997; Gourbesville, 2000; Chaboche et al., 2012). This material is known to exhibit cyclic softening in relation to the shearing of precipitates during plasticity. Up to 600 °C, the yield stress and ultimate tensile stress are quite stable. Inconel 718 also has important ductile behavior. Maximal deformation at failure reaches 18 % during tensile tests at room temperature. Dynamics tests, performed at room temperature, have proven that this material is sensitive to strain rate variations (Lee et al., 2011; Wang et al., 2013). More specifically, for strain rates greater than 1000 s^{-1}, the yield stress increases significantly. Based on this literature review, the chosen constitutive model is an elasto-visco-plastic model proposed by Chaboche et al. (2012). In this model, the total strain tensor ϵ is additively decomposed into the elastic ϵ^e and plastic ϵ^p strain tensors. The elastic domain is defined by $f \leq 0$ in the stress space σ with:
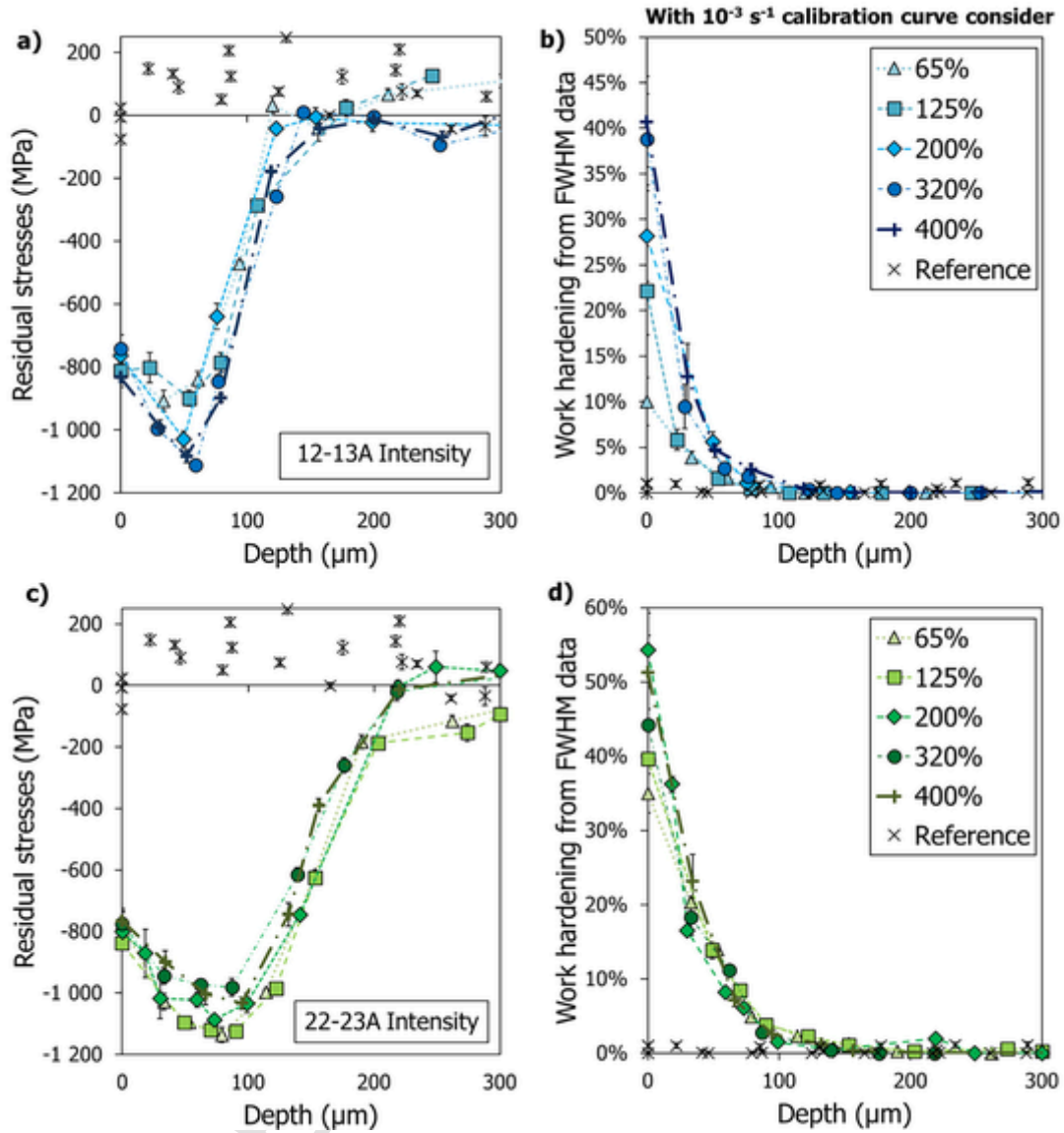
Fig. 6. Experimental residual stresses (a-c) and work hardening (b-d) profiles as a function of depth for various coverage and two fixed Almen intensity F12-13A (in blue) and F22-23A (in green). Work hardening is calculated from the 10^{-3} s^{-1} calibration curve shown in Fig. 4. (For interpretation of the references to colour in this figure legend, the reader is referred to the web version of this article.)

$$f = J(\sigma - X) - R \tag{2}$$

where the function J returns the von Mises invariant, R indicates the size of the instantaneous yield condition and X is the back stress tensor. The plastic strain rate tensor $\dot{\varepsilon}^p$ is obtained with the flow rule, using the normality assumption:

$$\dot{\varepsilon}^p = \lambda \frac{\partial f}{\partial \sigma} \tag{3}$$

where the dot represents the differentiation with respect to time. To model strain rate effects, the plastic multiplier λ is given by the Norton power law:

$$\lambda = \left\langle \frac{f}{K} \right\rangle^n \tag{4}$$

The equivalent plastic strain rate $\dot{p}$ is:

$$\dot{p} = \sqrt{\frac{2}{3}\dot{\varepsilon}^p : \dot{\varepsilon}^p} \tag{5}$$

A non-linear isotropic hardening R is defined as the sum of several contributions indexed with "i":

$$R = \sum_i R^i \text{ with } \dot{R}^i = b_i \left(Q_i - R^i \right) \dot{p} \tag{6}$$

where the b_i and Q_i are material parameters associated to contribution i. Similarly, the back stress X is decomposed as the sum of several contributions, indexed with "k":

$$X = \sum_k X^k \tag{7}$$

with:

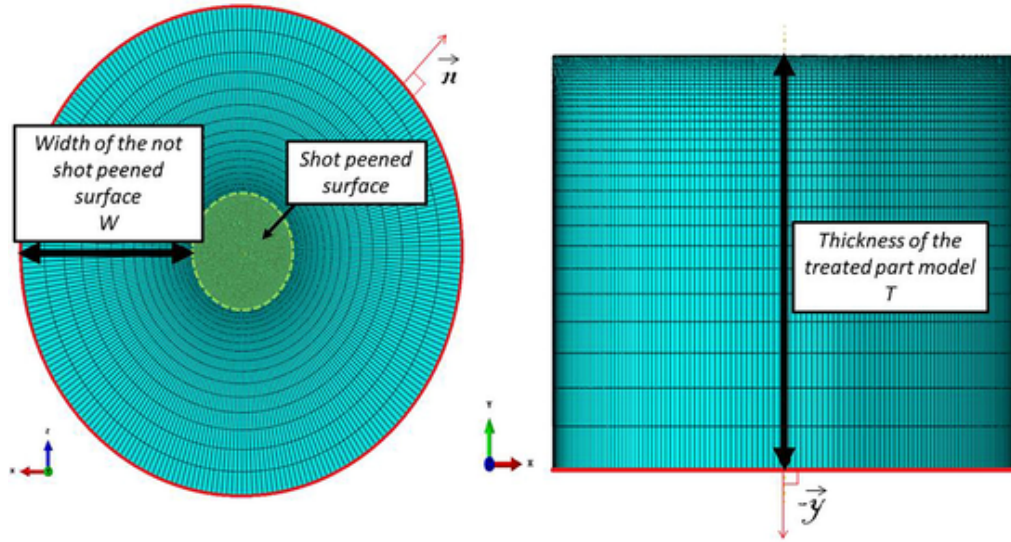$$\dot{X}^k = \frac{2}{3}C_k\dot{\varepsilon}^p - D_k X^k\dot{p} \tag{8}$$

Fig. 7. Dimensions of the finite-element model of treated part model.
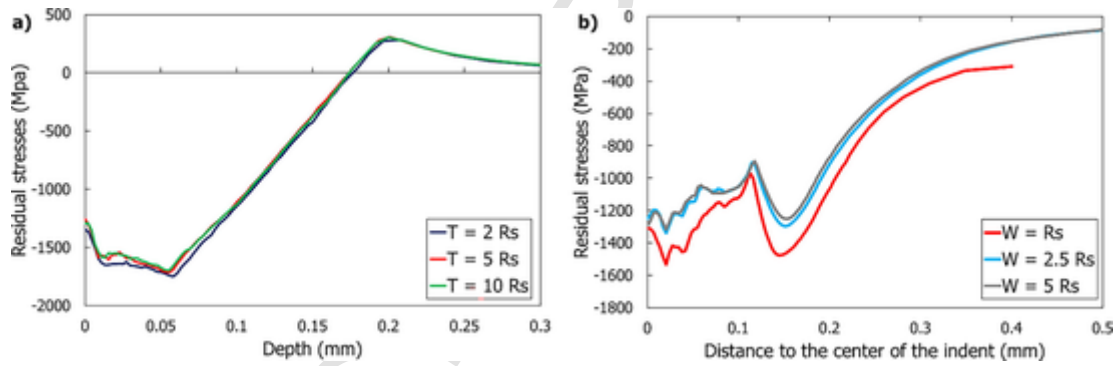

Fig. 8. Residual stresses observed as a function of treated part dimensions: along the depth (a) and along the radius at the surface (b). T: thickness of the treated part, W: width of the not shot peened zone and R_s: radius of the shot.

Table 5
Mean, minimum and maximum values of strain rates during shot peening for three elements located at a position (x,y) in the bulk and a depth z = 0, 50 and 100 μm at the surface.

Element depth	Minimal strain rate (s^{-1})	Average strain rate (s^{-1})	Maximal strain rate (s^{-1})
z = 0 μm	7	42,850	766,000
z = 50 μm	3	12,400	128,000
z = 100 μm	0.3	2625	13,600

where C_k, D_k are material parameters associated to each contribution k.

The parameters identified for IN718 DA at room temperature are listed in Table 5.

4.4. Coverage model

When multi-impact modeling is performed, several strategies can be considered to distribute the impacts on the surface of the part: impacts can be distributed randomly as proposed by Miao et al. (2009), or using the symmetry cells method (Bagherifard et al., 2012b; Zimmermann et al., 2010). Based on the experimental observations described in Section 3, it was chosen to randomly position the impacts using a normal distribution.

Due to the randomness of the position of the impacts, a methodology to evaluate the coverage had to be implemented. Three different methods to assess the coverage of the finite element model have been considered. They are described and compared in the following paragraph. For each method, full coverage is considered to be achieved when a coverage of 98 % is reached.

The first method is based on a model proposed by Avrami (1941). This model assumes that the impacts leave a perfect circular dimple on the treated surface. Thus, the coverage percentage A_c is given by:

$$A_c = 100 \left[1 - exp \left(-\pi R_d^2 \frac{N_i}{S_T} \right) \right] \qquad (9)$$

where R_d is the radius of the dimple, N_i the number of spheres having impacted the surface and S_T the total impacted surface. The Avrami model gives an instant estimation of the coverage as a function of the number of spheres impacting the surface, but does not take into account the real geometry of the dimple, neither the hardening of the material during the process.

The second method implemented is the one proposed by Gangaraj et al. (2014). With this method, coverage is evaluated by considering the cumulated plastic strain at the surface of the treated material. The first step consists of the definition of a plastic strain threshold, evaluated at the boundary of the plastic dimple left by a unique shot on a plane surface, as shown in Fig. 9.a. For an incident shot velocity of 75 m.s^{-1} and 40 m.s^{-1}, the plastic threshold has been found to be 0.036 and 0.034 re-
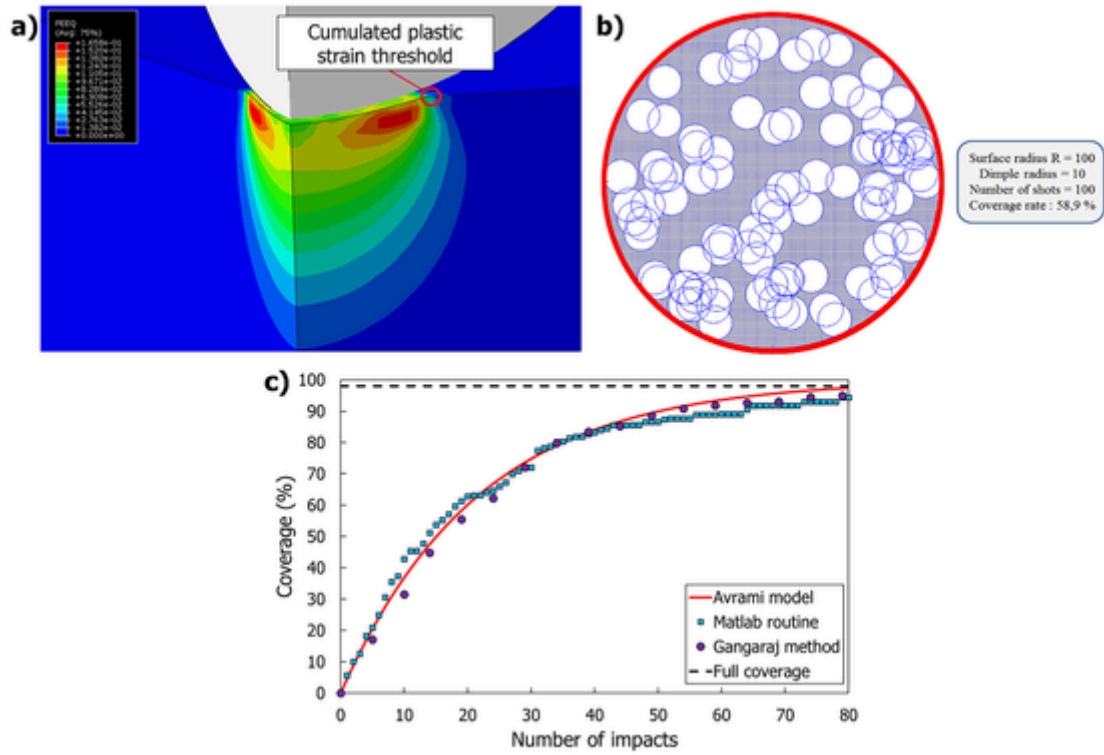
Fig. 9. a) Evaluation of the plastic threshold from a single impact simulation. b) Illustration of matlab routine coverage assessment. c) Comparison of three methods for coverage assessment of numerical simulations.
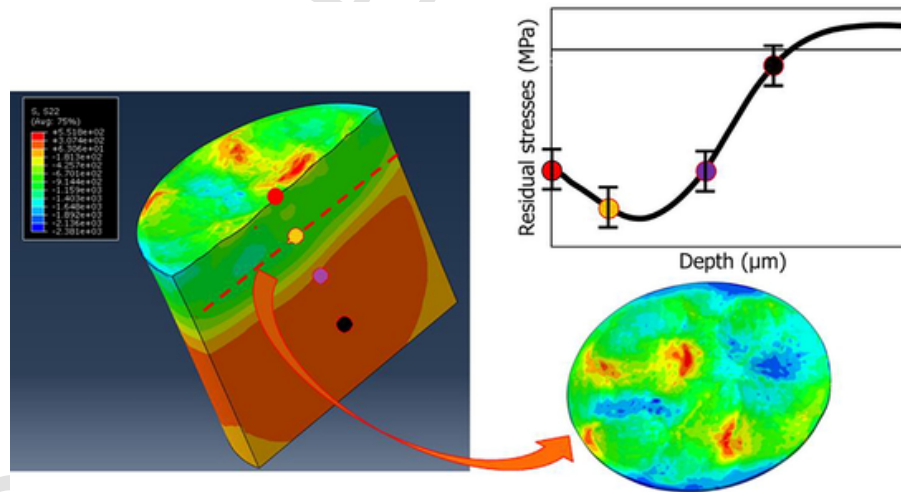

Fig. 10. Illustration of the extraction and averaging methodology for numerical data.

spectively. Thus, the criterion is assumed to be independent of the velocity in this study and set to 0.035. Plastic deformation of surface elements of the model has been compared to this threshold. If equal or superior, the corresponding element is declared as covered. Assessment of the coverage has been performed during the simulation with an evaluation of the ratio between the number of covered elements and the total number of elements on the surface.

The third method implemented is a Matlab routine specifically implemented by the authors. The routine consists of recording the random position of the impacts during the simulation of the process. It is assumed that the footprint is identical for all the impacts and equal to the area corresponding to a single impact test under similar conditions. This area is then assigned to the coordinates of each recorded impact.

Coverage is then evaluated as the ratio between the area of the impacted surface and the total shot peened surface. Fig. 9.b presents an example of the resulting coverage obtained with such a methodology.

Fig. 9.c compares the three methods previously presented for an Almen intensity of *F22-23A*. It is quite satisfactory to conclude that all the methods converge to the same number of spheres needed to achieve full coverage. It can be concluded that these three methods can be used indifferently. For practical reasons, the Matlab routine has been used hereafter.
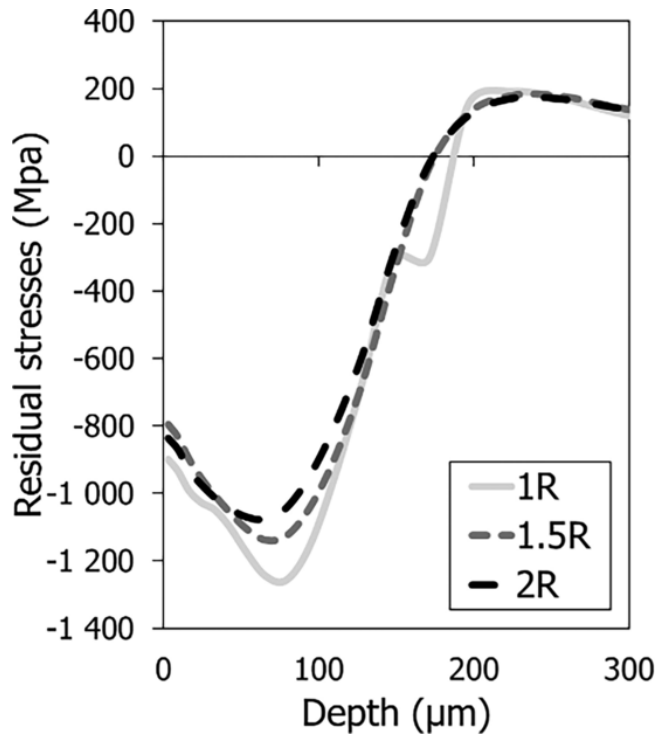
Fig. 11. Comparison of numerical results for three values of the area of shot-peened surface. Shot peening condition: F22-23A, 100% coverage.

5. Analysis of the numerical results

This section presents preliminary analysis of the simulated results that have been conducted to validate the model proposed in the previous section. It also details specific treatments of the data for comparison with experimental measurements.

5.1. Average and standard deviation for computed residual stresses and work hardening

The solution fields obtained with the numerical simulation present some spatial heterogeneity (see Fig. 10). A specific treatment has been performed on the numerical data to be able to compare the residual stresses and work hardening obtained with the simulations to the experimental result. The variables of interest, the residual stresses σ_{xx} and the equivalent plastic strain ε^p, have been extracted and averaged to a depth equivalent to the material's X-ray penetration. In our case, this penetration was estimated to be between 2 and 4 μm. Hence, in order to constitute one point on the numerical profile, the average and the standard deviation of the values of interest were computed on elements over a depth of 8 μm, value of the same order of magnitude, chosen to allow an optimization between the experimental value obtained by XRD and the size of the elements of the model, themselves optimized to reduce the calculation time. Each thickness considered for the calculation of average and standard deviation values represents more than 8000 elements. This methodology is illustrated in Fig. 10. This extraction ensures consistency with the experimental results, and also provides information on the mechanical states that can be observed at the scale of an element (a few micrometers). The objective of this section is thus also to analyze the distribution of the residual stresses and the work hardening as a function of depth in the solid. For these studies, three coverage values have been imposed: *65 %*, *125 %* and *200 %* with the Almen intensity set to *F22-23A*.

The choice of the radius of the cylinder on which the average data is based requires particular attention: it has to be chosen for the results to be representative of shot peening (Gariépy et al., 2011; Mylonas and Labeas, 2011; Kim et al., 2012). A comparison of averaged profiles was therefore conducted by varying the value of the area of shot-peened surface with radii of R_s, $1.5R_s$, and $2R_s$, where R_s is the radius of the shot. These results, presented in Fig. 11, show that for a studied part of radius $1R_s$, the averaged stress profile presents fluctuations that do not appear for the other two profiles. For this same radius, we can also see that the maximal residual stress is much more pronounced. These observations suggest that a cylinder of $1R_s$ is too small to obtain a homogeneous mechanical state after shot peening simulation. On the other hand, a radius of $1.5R_s$ is sufficient and corresponds to the value that has been used in the present study.
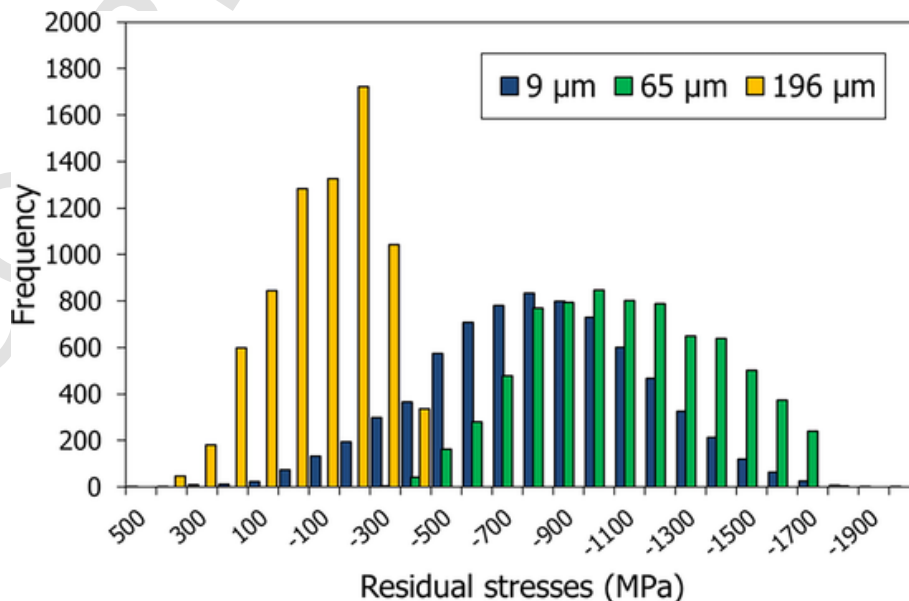

Fig. 12. Residual stress distribution for different depths (9 μm, 65 μm and 196 μm) after shot peening simulation (F22-23A intensity, 125 % coverage).
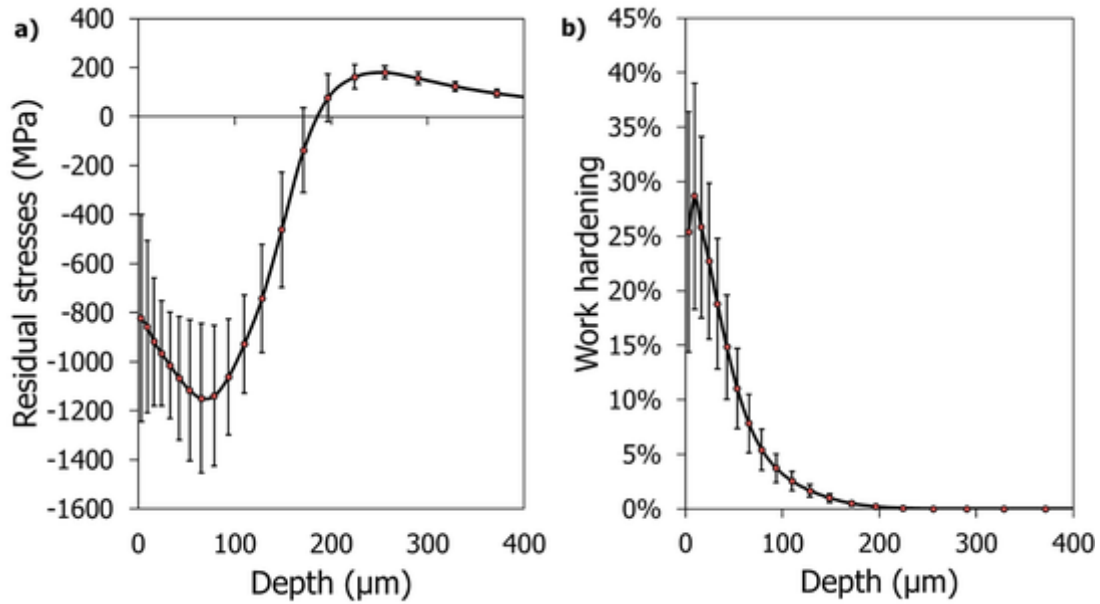
Fig. 13. Residual stresses (a) and work hardening (b) profiles, and associated standard deviations obtained after numerical simulation of shot peening condition 22-23A, 125%.

The distribution of residual stresses for three given depths is extracted (9 μm, 65 μm and 196 μm) and presented in Fig. 12 for a coverage of *125 %*. A Gaussian shape is observed for the distribution at each depth. A mean value is computed for each depth. These results also indicate that the width of the distribution depends on the selected depth. A similar analysis can also be performed for work hardening. The average and standard deviations of the residual stresses and work hardening have been calculated for each depth of the massif. Fig. 13 presents the evolution of the average of the residual stresses and work hardening as a function of depth with the standard deviation bars associated with each depth. The higher the levels of residual stresses and work hardening, the higher the associated standard deviations.

Experimental data concerning the dispersion of the mechanical state after shot peening (Vöhringer, 1987) are scarce but corroborate the results presented here. Vöhringer measured the residual stresses on the surface of a shot peened sample at 11 different locations by X-ray diffraction. A collimator size of the same order of magnitude as the numerically analyzed area was used to perform the measurements, which allows comparison of the results with this numerical study. Vöhringer observed that the compressive residual stresses ranged from −180 to −500 MPa, with an average of −370 MPa. Although the shot peening conditions were different from the one used in this work, these results, show that the significant variations in the mechanical state are physical. Similar results have recently been obtained numerically (Daoud et al., 2021).

Fig. 14 presents the evolution of the standard deviation as a function of depth for residual stresses (a) and work hardening (b) for the three coverages investigated. As seen before, a notable evolution is observed in the depth. The results are very similar for the three coverages. These results indicate that the standard deviations are thus only slightly dependent on the shot peening conditions applied in the model. In the following, for readability reasons, the numerical error bars are not presented in the figures when numerical results are compared to the experimental data (Section 6). Another representation of the results by normalizing Fig. 14.a and Fig. 14.b by the mean stress and work hardening calculated at each depth and for each shot peening condition respectively provides further information (Fig. 14.c and Fig. 14.d). It can be observed that the maximum errors are not located near the surface but located when the stress is almost equal to zero.

The same conclusion can be drawn for residual stresses and work hardening.

5.2. Mechanical state within the massif

In order to validate the modeling, a first analysis concerning the over-all distribution of the residual stress and plastic strain fields is performed. For these studies, the coverage is *125 %* with the Almen intensity set to *F22-23A*. The different components of the residual stress and plastic strain tensors are presented in Fig. 15 as a function of depth. The raw numerical results have been averaged as presented in Section 5.1. The general shape of these tensors corresponds to what is expected after a shot peening treatment:

- The components, σxx and σzz of the residual stress are nearly identical beyond 40 μm in depth.
- The shear stress components, σxy, σxz and σyz, are very low, on the order of a few tens of MPa.
- The plastic strain tensor is of zero trace (less than 5.10^{-9}).

Some differences with the expected results are observed on the first tens of microns. The strains ε_{pzy} are also non-negligible in this superficial part of the bulk. Also, the shear components of the residual stress tensor are non-zero for this thickness. For these depths, no conclusion may be drawn because the numerical results are reported in the local reference system in a volume where the elements are highly deformed.

5.3. Evolution of the strain rate within the massif

It has been observed that the experimental calibration of work hardening is dependent on the strain rate (see Fig. 4 and Goulmy et al., 2021b, 2021a). The knowledge of the strain rate variations in the bulk of the material during shot peening is thus, ideally, necessary to use the calibration curves.

During the shot peening treatment, the strain rate changes with time and depth. The numerical analysis gives access to the local value of the strain rate.

Consider a simulation for the Almen intensity that induces the highest strain rates studied here (*F22-23A*). Three elements located at an ar-
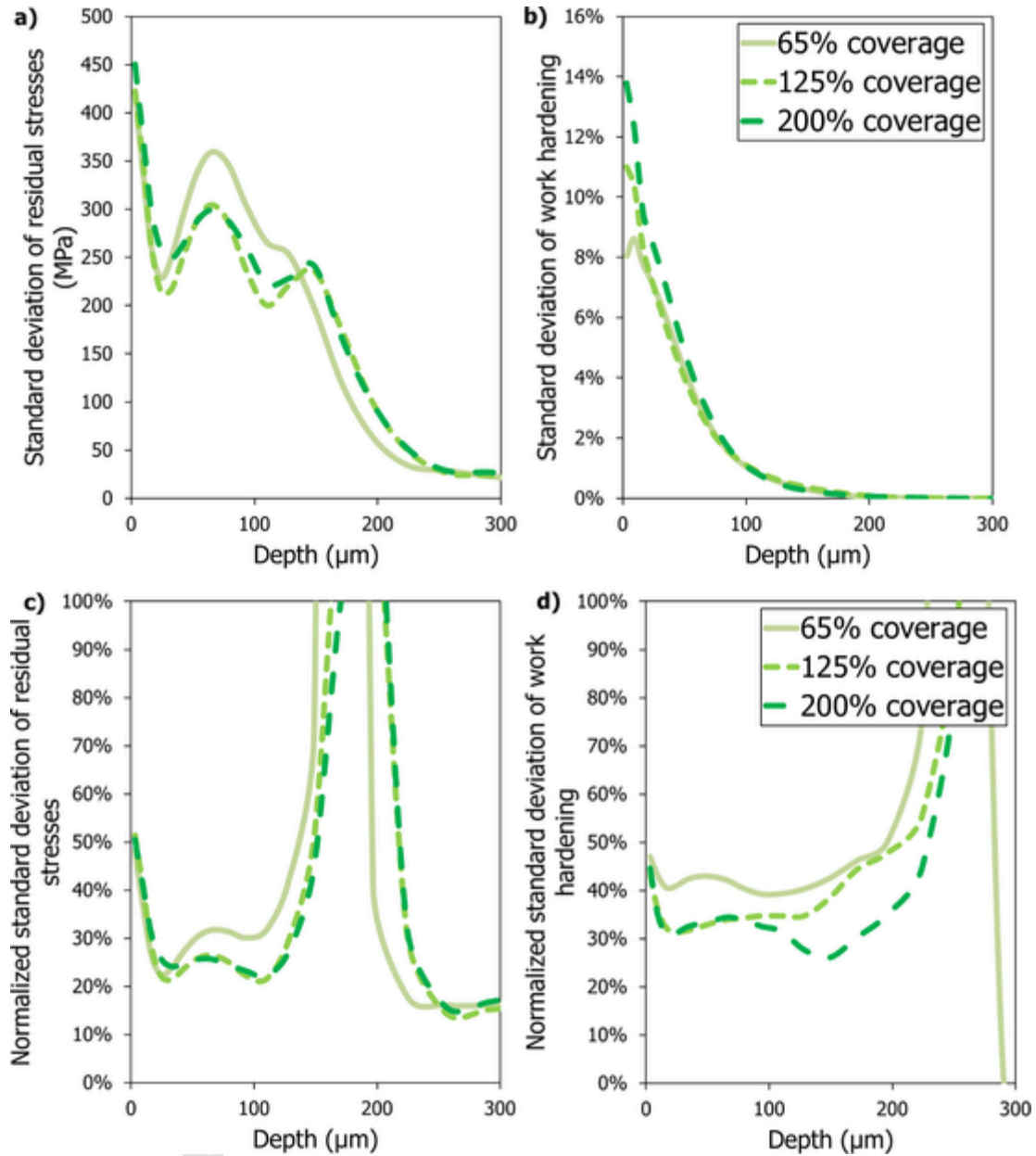
Fig. 14. Numerical deviation profile along depth for residual stresses (a) and work hardening (b). Normalized standard deviation of numerical profile along depth for residual stresses (c) and work hardening (d). V = 65 m.s^{-1} and D = 345 μm, both parameters are constant.

bitrary position (x,y) on the massif have been selected at depths: z = 0, 50 and 100 μm. The average, minimal and maximal strain rates obtained during the simulation for these three elements are presented in Table 5. The average strain rate value is calculated by averaging the strain rates computed for each depth during the shot peening process. As expected, the strain rates are not homogeneous in-depth.

These results indicate the difficulties encountered in comparing the experimental and simulated data. We propose here a methodology to achieve this comparison using the calibration curves at a given strain rate as an upper or lower limit for the work hardening in the depth induced in the material. In the following, it is then proposed to frame the work hardening values obtained with the help of modeling with the experimental results calibrated for two extreme strain rates, 10^{-3} s^{-1} and 10^3 s^{-1}.

6. Comparison with experimental results

The objective of this section is to present a detailed comparison of the results obtained with the numerical solutions from the model presented in Section 4 and the experimental results presented in Section 3. In particular, the model is tested on its ability to reproduce accurately the influence of the Almen intensity and the coverage on the residual stress and work hardening profiles. The different model conditions that have been investigated are presented in Table 2.

It has been observed (see Section 5.3) that the strain rates within the material vary both in time, during the shot peening process and in space, as a function of depth. It has also been observed (see discussion, Section 2.4) that the strain rate has an influence on the experimental calibration to evaluate work hardening. This is why we must compare the numerical results with the hardening values obtained with both the calibration curves for 10^{-3} s^{-1} and 10^3 s^{-1} (curves depicted in Fig. 4).
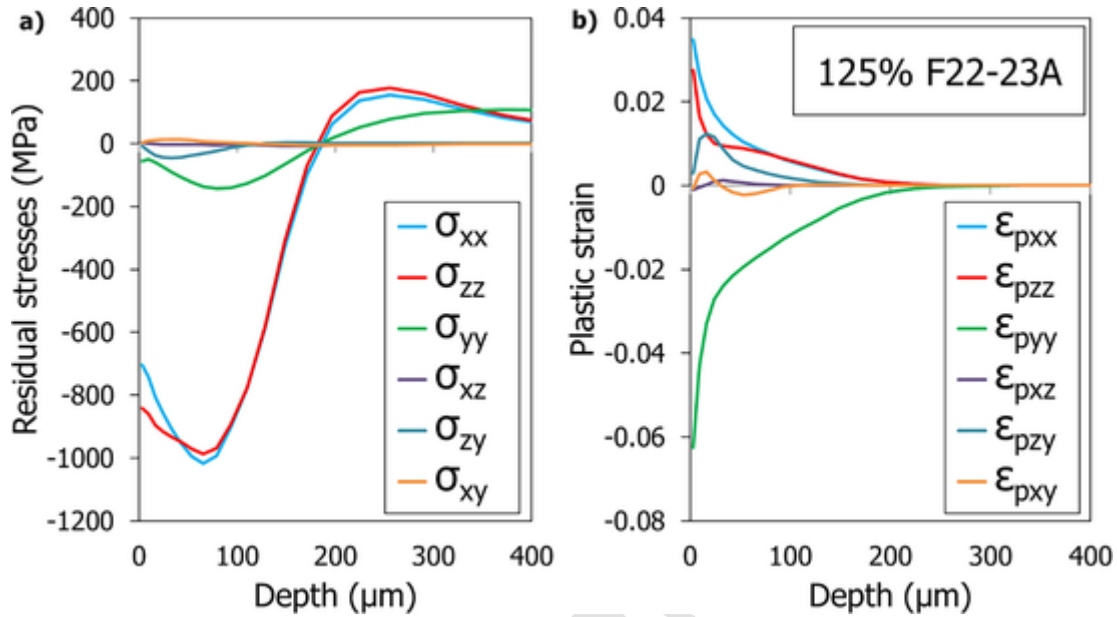
Fig. 15. Comparison of residual stress (a) and plastic strain (b) components as a function of depth (F22-23A intensity, 125% coverage).

6.1. Almen intensity influence

The influence of the Almen intensity on the residual stress field and hardening state is presented in Fig. 16 for the model (lines) and the experimental results (symbols). For this part, the coverage was set to *200 %*. The only parameter that differs between each simulation is the average velocity of the shot corresponding to the three Almen intensities: *F12-13A*, *F17-18A* and *F22-23A*.

Overall, the experimental results are well reproduced by the model. An increase in Almen intensity induces little change in surface residual stresses, whereas it induces an increase in the depth affected by compressive residual stresses and a shift of the compressive peak toward the interior of the part. From a more quantitative point of view, the surface values as well as the compression peak predicted by the model are in good agreement with the experiment for all the Almen intensities. The depth affected by the residual stresses is also well predicted, with differences between the model and the experiment lower than 30 μm.

Concerning work hardening, the model is again predictive. An increase in Almen intensity induces an increase in surface work hardening and has little impact on the affected depth. The results obtained at the surface are particularly interesting. Indeed, when the 10^{-3} s^{-1} calibration curve is considered to evaluate the work hardening experimentally, the model predicts values below those estimated experimentally. This was expected since the strain rates encountered at the surface of the parts during shot peening are much higher than these strain rates (see Table 5). Thus, the model is accurate when compared to the values obtained experimentally at strain rates of 10^3 s^{-1}, especially for higher intensity (*F22-23A*). It therefore appears judicious to preferentially consider the experimental data obtained with this specific calibration curve (corresponding to a strain rate of 10^3 s^{-1}) when considering the results close to the surface. On the other hand, beyond a depth of 30 μm, the strain rates generated during the impacts are lower (see Table 5). It is then preferable to consider a calibration curve obtained at a lower strain rate.

6.2. Coverage influence

The influence of the coverage on the residual stress and work hardening profiles is presented in Fig. 17 and Fig. 18 for an Almen intensity of *F12-13A* and *F22*-23A respectively. Consider first the intensity of *F12-13A*. The correspondence between the experiment and the simula-

tion is quite satisfactory for the residual stress profiles corresponding to a coverage of *65 %* and *200 %*. On the other hand, differences are observed for the profiles corresponding to a coverage of *125 %*, especially concerning the depth affected by the shot peening. For this coverage value, the affected depth is 50 μm lower than the experimental data. This result appears rather surprising, it was not possible to identify the origin. Further investigations would be necessary. Concerning work hardening, the numerical results are in good agreement with the experimental data beyond a depth of 50 μm. As previously explained, the experimental results are closer when the calibration curve corresponding to the strain rate of 10^{-3} s^{-1} is used to evaluate the work hardening experimentally, except at the surface where a higher strain rate has to be considered.

Consider now the Almen intensity of *F22-23A* (Fig. 18). Again, the three coverages (*65 %*, *125 %* and *200 %*) have been investigated. Overall, the numerical results are in agreement with the experimental observations. The surface residual stresses are independent of the coverage value; the affected depth and the maximal compressive residual stresses fluctuate slightly with no direct relation to the coverage value. Quantitatively, the surface residual stresses are also well reproduced. On the other hand, the maximal compressive residual stresses are slightly underestimated (100 MPa) and the affected depth is also underestimated by about 50 μm for the *65 %* and *125 %* coverage. The experimental evaluation of the work hardening levels is also well reproduced by the model. An increase in the coverage leads to an increase in surface work hardening and no evolution of the work hardened depth. As before, the numerical values are contained within the experimental measurement set up with the calibration. The results are in very good agreement beyond 40 μm depth.

7. Conclusion

In order to assess the influence of shot peening conditions on the creation of residual stress and work hardening on IN718 DA, a comprehensive model for shot peening has been proposed. The originality of this model lies in the consideration of the work hardening induced by the shot peening process. The validation of this model has been performed through specific experimental characterization of various shot peening treatments conducted on parallelepipedic samples. The influence of Almen intensity and coverage on mechanical fields has been investigated. For each shot peening condition, the residual stress profiles
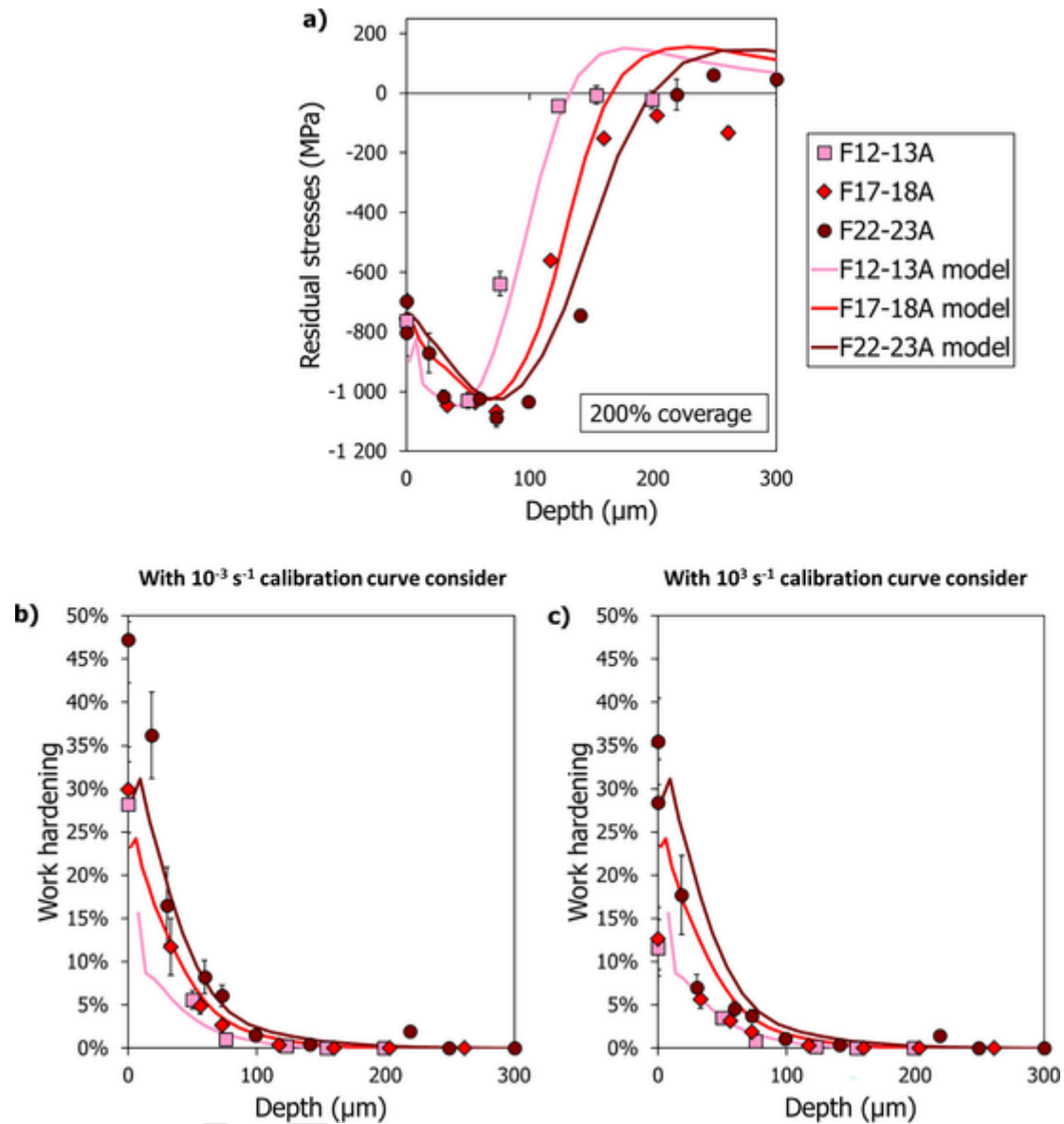
Fig. 16. Comparison between numerical and experimental profiles of residual stresses (a), and work hardening estimated with a calibration curve using a 10^{-3} s^{-1} strain rate (b) and (c) with a calibration curve using a 10^3 s^{-1} strain rate, for different Almen intensity (F12-13A, F17-18A, F22-23A). Coverage was fixed to 200 %.

but also the work hardening profiles in the depth of the sample have been determined. The numerical model proposed in this work has demonstrated its ability to reproduce a wide range of shot peening conditions.

The model is able to predict the work hardening level in shot peened parts and in particular:

- For a fixed coverage, an increase in Almen intensity mainly influences the depth affected by the compressive residual stress. The maximum compressive residual stress changes slightly. On the contrary, work hardening exhibits a constant growth with shot peening intensity. This growth is more important at the surface.
- For a fixed peening intensity, an increasing coverage values does not affect the residual stresses profiles, whatever the coverage. On the other hand, work hardening increases constantly until it reaches a stabilized value for coverage values above 200 %.

This work opens the possibility to create a chain from process modeling to fatigue life prediction of parts by taking into account both residual stresses and work hardening. It is now possible to use this model to evaluate the influence of the dispersion of the process parameters on the mechanical fields or to estimate the residual mechanical fields in the case of more complex parts such as gears or corners.

Declaration of Competing Interest

The authors declare that they have no known competing financial interests or personal relationships that could have appeared to influence the work reported in this paper.

Data availability
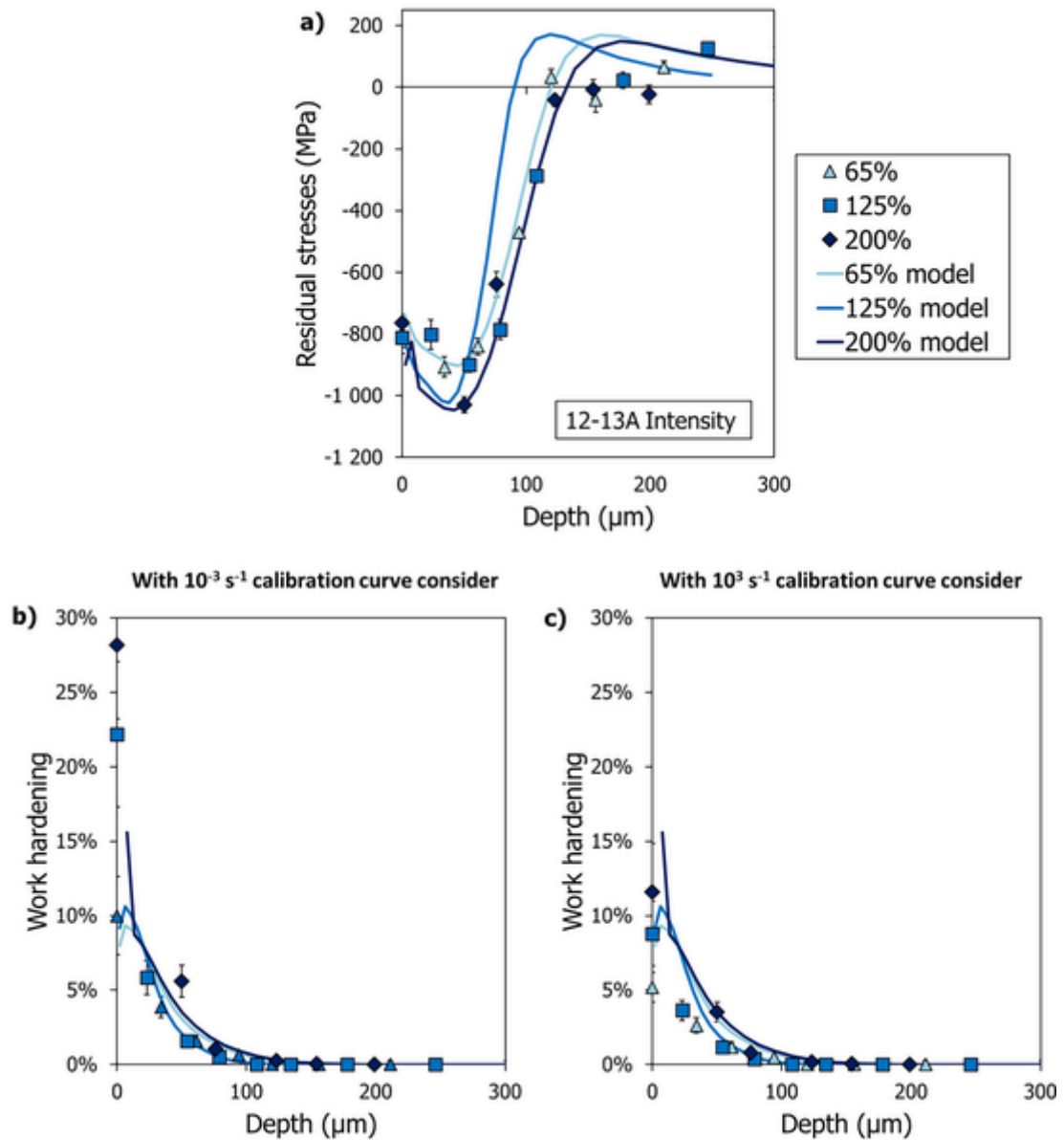
Data will be made available on request.

Fig. 17. Comparison between numerical and experimental profiles of residual stresses (a) and work hardening (b) and (c), for different coverage (65%, 125%, 200%). Almen intensity was fixed to F12-13A.
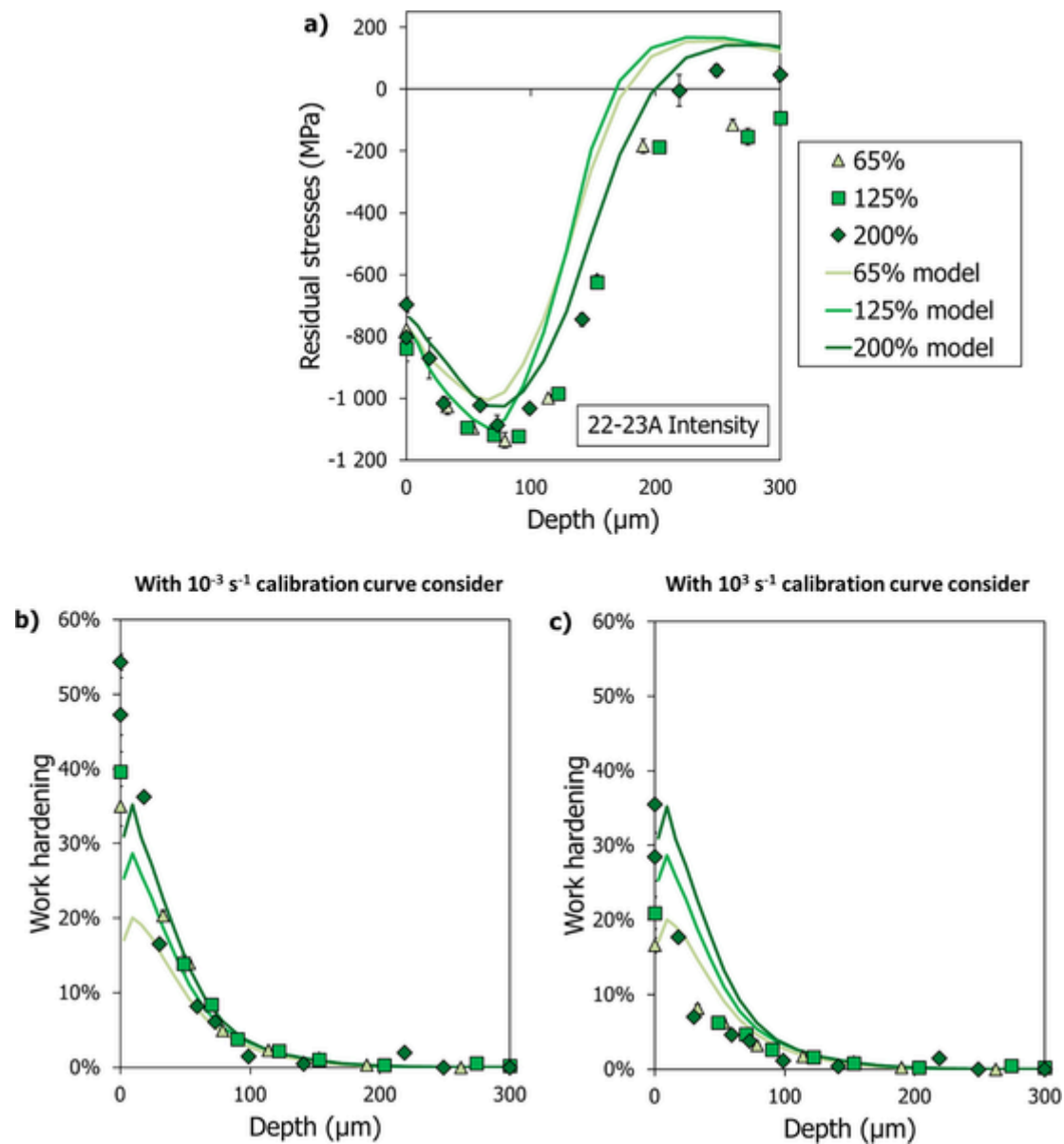
Fig. 18. Comparison between numerical and experimental profiles of residual stresses (a) and work hardening (b) and (c), for different coverage (65%, 125%, 200%). Almen intensity was fixed to F22-23A.

References

Al Baida, H., Kermouche, G., Langlade, C., 2015. Development of an improved method for identifying material stress–strain curve using repeated micro-impact testing. Mech. Mater. 86, 11–20. https://doi.org/10.1016/j.mechmat.2015.02.009.

Alexandre, F., Deyber, S., Pineau, A., 2004. Modelling the optimum grain size on the low cycle fatigue life of a Ni based superalloy in the presence of two possible crack initiation sites. Scr. Mater. 50, 25–30. https://doi.org/10.1016/j.scriptamat.2003.09.043.

Al-Hassani, S., 1981. Mechanical aspects of residual stress development in shot peening. Shot Peening 583.

Avrami, M., 1941. Geometry and dynamics of populations. Philos. Sci. 8, 115–132. https://doi.org/10.1086/286681.

Bagherifard, S., Ghelichi, R., Guagliano, M., 2012a. Numerical and experimental analysis of surface roughness generated by shot peening. Appl. Surf. Sci. 258, 6831–6840. https://doi.org/10.1016/j.apsusc.2012.03.111.

Bagherifard, S., Ghelichi, R., Guagliano, M., 2012b. On the shot peening surface coverage and its assessment by means of finite element simulation: A critical review and some original developments. Appl. Surf. Sci. 259, 186–194. https://doi.org/10.1016/j.apsusc.2012.07.017.

Bagherifard, S., Ghelichi, R., Guagliano, M., 2014. Mesh sensitivity assessment of shot peening finite element simulation aimed at surface grain refinement. Surf. Coat. Technol. 243, 58–64.

Baragetti, S., 2001. Three-dimensional finite-element procedures for shot peeening residual stress filed prediction. Int. J. Comput. Appl. Technol. 14 (1/2/3), 51.

Chaboche, J.L., Jung, O., 1997. Application of a kinematic hardening viscoplasticity model with thresholds to the residual stress relaxation. Int. J. Plast 13, 785–807. https://doi.org/10.1016/S0749-6419(97)00066-1.

Chaboche, J.-L., Kanouté, P., Azzouz, F., 2012. Cyclic inelastic constitutive equations and their impact on the fatigue life predictions. Int. J. Plast 35, 44–66. https://doi.org/10.1016/j.ijplas.2012.01.010.

Daoud, M., Kubler, R., Bemou, A., Osmond, P., Polette, A., 2021. Prediction of residual stress fields after shot-peening of TRIP780 steel with second-order and artificial neural network models based on multi-impact finite element simulations. J. Manuf. Process. 72, 529–543. https://doi.org/10.1016/j.jmapro.2021.10.034.

ElTobgy, M.S., Ng, E., Elbestawi, M.A., 2004. Three-dimensional elastoplastic finite element model for residual stresses in the shot peening process. Proc. Inst. Mech. Eng. B J. Eng. Manuf. 218, 1471–1481. https://doi.org/10.1243/0954405042418419.

François, M., Dionnet, B., Sprauel, J.M., Nardou, F., 1995. The influence of cylindrical geometry on X-ray stress tensor analysis. I. General formulation. J. Appl. Cryst. 28, 761–767. https://doi.org/10.1107/S0021889895006868.

François, M., Lebrun, J.-L., 1992. X-ray stress determination on materials with large size cristallites - theoretical approach. Proceedings of the 3rd European Conf. on Residual Stress.

Gangaraj, S.M.H., Guagliano, M., Farrahi, G.H., 2014. An approach to relate shot peening finite element simulation to the actual coverage. Surf. Coat. Technol. 243, 39–45.

Gariépy, A., Larose, S., Perron, C., Lévesque, M., 2011. Shot peening and peen forming finite element modelling – Towards a quantitative method. Int. J. Solids Struct. 48, 2859–2877. https://doi.org/10.1016/j.ijsolstr.2011.06.003.

Goulmy, J.P., Kanoute, P., Rouhaud, E., Toualbi, L., Kruch, S., Boyer, V., Badreddine, J., Retraint, D., 2021a. A calibration procedure for the assessment of work hardening Part II: Application to shot peened IN718 parts. Mater. Charact. 175, 111068. https://doi.org/10.1016/j.matchar.2021.111068.

Goulmy, J.P., Rouhaud, E., Kanoute, P., Toualbi, L., Kruch, S., Boyer, V., Badreddine, J., Retraint, D., 2021b. A calibration procedure for the assessment of work hardening part I: Effects of the microstructure and load type. Mater. Charact. 175, 111067. https://doi.org/10.1016/j.matchar.2021.111067.

Gourbesville, O., 2000. Caractérisation par DRX de la microstructure d'alliages à base de nickel (718) et à base de titane (Ti-17) forgés et traités, prévision des propriétés mécaniques (Thèse de doctorat). Arts et Métiers ParisTech, France.

Guagliano, M., 2001. Relating Almen intensity to residual stresses induced by shot peening: a numerical approach. J. Mater. Process. Technol. 110, 277–286. https://doi.org/10.1016/S0924-0136(00)00893-1.

Hasegawa, N., Watanabe, Y., Fukuyama, K., 1996. Creation of residual stress by high speed collision of a steel ball. JSSP, Symposium on Recent Research Of Shot Peening 1–7.

J2277: Shot Peening Coverage Determination - SAE International, n.d.

Kermouche, G., Grange, F., Langlade, C., 2013. Local identification of the stress–strain curves of metals at a high strain rate using repeated micro-impact testing. Mater. Sci. Eng. A 569, 71–77. https://doi.org/10.1016/j.msea.2013.01.020.

Kim, T., Lee, H., Kim, M., Jung, S., 2012. A 3D FE model for evaluation of peening residual stress under angled multi-shot impacts. Surf. Coat. Technol. 206, 3981–3988. https://doi.org/10.1016/j.surfcoat.2012.03.078.

Klemenz, M., Schulze, V., Rohr, I., Löhe, D., 2009. Application of the FEM for the prediction of the surface layer characteristics after shot peening. J. Mater. Process. Technol. 209, 4093–4102. https://doi.org/10.1016/j.jmatprotec.2008.10.001.

Kobayashi, M., Matsui, T., Murakami, Y., 1998. Mechanism of creation of compressive residual stress by shot peening. Int. J. Fatigue 20, 351–357. https://doi.org/10.1016/S0142-1123(98)00002-4.

Kubler, R.F., Rotinat, R., Badreddine, J., Puydt, Q., 2020. Experimental analysis of the shot peening particle stream using particle tracking and digital image correlation techniques. Exp. Mech. 60 (4), 429–443.

Lee, W.-S., Lin, C.-F., Chen, T.-H., Chen, H.-W., 2011. Dynamic mechanical behaviour and dislocation substructure evolution of Inconel 718 over wide temperature range. Mater. Sci. Eng. A 528, 6279–6286. https://doi.org/10.1016/j.msea.2011.04.079.

Majzoobi, G.H., Azizi, R., Alavi Nia, A., 2005. A three-dimensional simulation of shot peening process using multiple shot impacts. J. Mater. Process. Technol. 164–165, 1226–1234.

Maliaris, G., Gakias, C., Malikoutsakis, M., Savaidis, G., 2021. A FEM-based 2D model for simulation and qualitative assessment of shot-peening processes. Materials 14, 2784. https://doi.org/10.3390/ma14112784.

Meguid, S., Sagals, G., Stranart, J.C., 2002. 3D FE analysis of peening of strain-rate sensitive materials using multiple impingement model. Int. J. Impact Eng. 27, 119–134. https://doi.org/10.1016/S0734-743X(01)00043-4.

Meguid, S.A., Shagal, G., Stranart, J.C., Daly, J., 1999. Three-dimensional dynamic finite element analysis of shot-peening induced residual stresses. Finite Elem. Anal. Des. 31, 179–191. https://doi.org/10.1016/S0168-874X(98)00057-2.

Miao, H.Y., Larose, S., Perron, C., Lévesque, M., 2009. On the potential applications of a 3D random finite element model for the simulation of shot peening. Adv. Eng. Softw. 40, 1023–1038. https://doi.org/10.1016/j.advengsoft.2009.03.013.

Mori, K., Osakada, K., Matsuoka, N., 1996. Rigid-plastic finite element simulation of peening process with plastically deforming shot. JSME Int. J. Ser. A, Mech. Mater. Eng. 39, 306–312. https://doi.org/10.1299/jsmea1993.39.3_306.

Mylonas, G.I., Labeas, G., 2011. Numerical modelling of shot peening process and corresponding products: Residual stress, surface roughness and cold work prediction. Surf. Coat. Technol. 205, 4480–4494. https://doi.org/10.1016/j.surfcoat.2011.03.080.

Norme AFNOR NFL 06-832, 1990.

Prevey, P.S., Hornbach, D.J., Mason, P.W., 1998. Thermal residual stress relaxation and distortion in surface enhanced GasTurbine engine components. ASM International.

Prevey, P.S., 2000. The effect of cold work on the thermal stability of residual compression in surface enhanced IN718. In: 20th ASM Materials Solutions Conference & Exposition. St. Louis, Missouri.

Rouhaud, E., Deslaef, D., 2002. Influence of shots' material on shot peening, a finite element model. Mater. Sci. Forum 404–407, 153–158. https://doi.org/10.4028/www.scientific.net/MSF.404-407.153.

Vöhringer, O., 1987. Changes in the state of material by shot peening. pp. 185–204.

Wang, X., Huang, C., Zou, B., Liu, H., Zhu, H., Wang, J., 2013. Dynamic behavior and a modified Johnson-Cook constitutive model of Inconel 718 at high strain rate and elevated temperature. Mater. Sci. Eng. A 580, 385–390. https://doi.org/10.1016/j.msea.2013.05.062.

Zhao, J., Tang, J., Zhou, W., Jiang, T., Liu, H., Xing, B., 2022. Numerical modeling and experimental verification of residual stress distribution evolution of 12Cr2Ni4A steel generated by shot peening. Surf. Coat. Technol. 430, 127993. https://doi.org/10.1016/j.surfcoat.2021.127993.

Zhou, J., Cui, K., Sun, Z., 2022. Peening-induced work hardening gradient and prediction of residual stress for a shot peened structure. Int. J. Solids Struct. 254–255, 111934.

Zhou, J., Sun, Z., 2022. Numerical characterization of shot peening induced work hardening gradient and verification based on FEM analysis. Int. J. Solids Struct. 244–245, 111586. https://doi.org/10.1016/j.ijsolstr.2022.111586.

Zimmermann, M., Klemenz, M., Schulze, V., 2010. Literature review on shot peening simulation. Int. J. Comput. Mater. Sci. Surf. Eng. 3, 289. https://doi.org/10.1504/IJCMSSE.2010.036218.